Physicochem. Probl. Miner. Process., 62(1), 2025, 217749

http://www.journalssystem.com/ppmp

Physicochemical Problems of Mineral Processing

ISSN 1643-1049

Selective depression of feldspar by carboxymethyl starch sodium in the flotation of quartz using polyether amine

Xianfeng Sun [1, 2], Yushan Bi [2], Yuying Li [2], Liuyin Xia [3], Hanyu Zhang [3], Shaowei Sun [4]

[1] State Key Laboratory of Mineral Processing, Beijing, China, 100160

[2] School of Chemistry and Chemical Engineering, Huanggang Normal University, Huanggang, Hubei, China, 438000

[3] Department of Chemical and Materials Engineering, University of Alberta, Edmonton, AB, Canada, T6G 1H9

[4] Henan GCL Silicon-based New Materials Co., Ltd, Zhumadian, Henan, China, 463000

Corresponding author: hanyu7@ualberta.ca (Hanyu Zhang)

Abstract: The selective flotation of quartz and feldspar under weakly alkaline conditions was investigated, with carboxymethyl starch sodium (CMS-Na) employed as a depressant and polyether amine (PEA) as a collector. Micro-flotation tests demonstrated that CMS-Na exhibited strong selective depression of feldspar while maintaining high quartz recovery. Optimal separation conditions were achieved at pH 9.0 with 30 mg/dm^3 CMS-Na and 4.0×10^{-4} mol/dm^3 PEA, resulting in feldspar recovery decreasing sharply to 12.51% while quartz recovery remained high at 92.17%. The selectivity index (SI) increased significantly from 3.03 to 9.07, highlighting enhanced separation efficiency. Spectroscopic analyses, including FTIR, Raman, and XPS, revealed that CMS-Na selectively adsorbed onto feldspar surfaces mainly via coordination with Al-sites, with a small portion additionally forming hydrogen bonds with -Al-OH or -Si-OH, effectively suppressing its flotation. Conversely, CMS-Na exhibited limited interaction with quartz, enabling subsequent PEA adsorption. XPS data further confirmed that PEA adsorption on quartz and feldspar occurs via electrostatic and hydrogen bonding interactions, with CMS-Na selectively inhibiting PEA adsorption on feldspar. These results underscore CMS-Na's role as an environmentally friendly and effective depressant, enabling efficient separation of quartz and feldspar without hazardous chemicals like hydrofluoric acid. This study offers a sustainable approach to mineral resource utilization in industrial applications.

Keywords: quartz, feldspar, flotation separation, carboxymethyl starch sodium (cms-na), polyether amine (pea), weakly alkaline conditions

1. Introduction

High-purity quartz (HPQ) is essential in various industries, including glass, ceramics, refractory materials, photovoltaics, and semiconductors (Minami et al., 2011; Santos et al., 2015; Teng and Wang, 2021). In 2023, the global HPQ market was valued at approximately USD 1.33 billion (Jaiswal, 2025). Asia-Pacific dominates the HPQ market, accounting for approximately 63% of the global share due to the rapid growth of the solar energy sector. China was a vital contributor for production of semiconductors, optical fibers, and other high-tech components. The HPQ (>99.99% SiO_2) is industrially processed from natural quartz deposits through a combination of mining, physical and chemical purification, and thermal treatment to remove impurities like Fe, Al, Ti, and Li (Pan et al., 2022). Of these processes, froth flotation is a critical step because it selectively removes impurities such as feldspar, mica, iron oxides, and other silicate minerals that were included in raw quartz ore (Shen et al., 2023; Sun et al., 2023).

In this course of separation, the challenges lie in the froth flotation of quartz from feldspar, because both share similar crystal structures and chemical compositions. The primary difference lies in the substitution

DOI: 10.37190/ppmp/217749

of 1/4 of the Si^{4+} ions in the quartz structure by Al^{3+} ions in feldspar. This substitution forms feldspar lattices composed of corner-sharing tetrahedra of AlO_4^{5-} and SiO_4^{4-}, connected in an infinite three-dimensional framework (Vidyadhar and Rao, 2007; Larsen et al., 2019). To compensate for the charge imbalance caused by the replacement of Si^{4+} with Al^{3+}, alkali metal ions such as K^+ and Na^+ are introduced into the corresponding tetrahedral structural units (Yin et al., 2012). As a result, they show very similar density (2.55-2.65 g/cm^3), closed hardness (Mohs hardness 6-7), and both exhibit negatively charged surface potentials.

To achieve quartz-feldspar froth flotation separation, historically, hydrofluoric acid (HF) was used as a quartz depressant. When the slurry contains 0.5-3.0% HF, approximately 0.5-3.0 kg/Mg of dosage, the pulp pH would be about 2.0. HF reacts with SiO_2 (quartz) to form fluosilicic acid and silicon tetrafluoride as shown in Eq. (1):

$$SiO_2 + 6HF = H_2SiF_6 + 2H_2O \quad (1)$$

The formation of fluosilicate ions (SiF_6^{2-}) dramatically changes quartz surface charge and its wettability, preventing its attachment to air bubbles. While the HF does not significantly affect feldspar because feldspar contains aluminum and alkali metal cations (K^+, Na^+, Ca^{2+}), which resist HF surface modifications (Larsen and Kleiv, 2016). Thus, amines have no strong interaction with the fluorinated quartz surface, making quartz stay in the sink while feldspar floats. The use of hydrofluoric acid (HF) in flotation raises serious environmental and safety concerns due to its toxicity, corrosiveness, and persistence in wastewater. Considering free fluoride (F^-) ions could bioaccumulate and cause long-term contamination, many countries strictly regulate HF discharge due to its environmental risks.

Researchers strive to develop fluorine-free froth flotation methods. For example, it is reported that under strong acid conditions, feldspar can be preferentially floated by using a mixed cationic and anionic collector (Vielra and Peres, 2007; Wang et al., 2016). Despite its advantages of being fluorine-free, the acidic processing poses challenges such as severe equipment corrosion and the need for effective treatment of acid-containing wastewater. Consequently, the fluorine-free technique for the separation of quartz and feldspar has a major focus on neutral pH. In the previous studies, organic acids, such as polysaccharides, oxalic acid, tartaric acid, and some bio-depressants such as tannins, proteins were adopted as depressants. The goal was to depress quartz and allow feldspar to float when the pulp pH was maintained between 4 and 8. Although separation was observed, the separation efficiency remained low. To achieve comparable depression for the HF processing, the organic acids or bio-depressant need to be used as high as 5-15 kg/Mg, which is obviously not cost-effective.

In this work, feldspar was depressed using carboxymethyl starch sodium, and polyether amine was utilized as the collector. This combination enables effective flotation separation of quartz and feldspar at pH 9, requiring significantly lower depressant dosages compared to organic acids or bio-depressants. This research advances fluorine-free flotation processes and offers a new direction for future studies in sustainable mineral processing.

2. Materials and methods

2.1. Materials

High-purity quartz and feldspar crystals employed in this work were sourced from Guangdong Province, China. After hand-picking, the lumps were comminuted in a zirconia ball mill. The 38-74 μm fraction was reserved for micro-flotation experiments, whereas the <38 μm fraction was milled further to <5 μm for zeta-potential, FTIR, Raman, and XPS measurements. XRD was conducted to determine the phase composition of the minerals, as shown in Fig. 1. The XRD patterns revealed no detectable secondary phases, confirming the mineralogical purity of both concentrates. Chemical composition data given in Table 1 show that the feldspar sample contained 14.56% K_2O and Na_2O, indicating it was a mixture of potassium feldspar and albite. The quartz sample exhibited a SiO_2 purity of 99.82%, with only trace impurities. These results verify the suitability of both samples for the subsequent micro-flotation experiments.

Table 1. Chemical compositions of mineral samples (wt.%)

Sample	SiO_2	K_2O	Na_2O	Al_2O_3	Fe_2O_3
Quartz	99.82	0.01	0.01	0.05	0.04
Feldspar	69.51	10.29	4.27	15.5	0.23

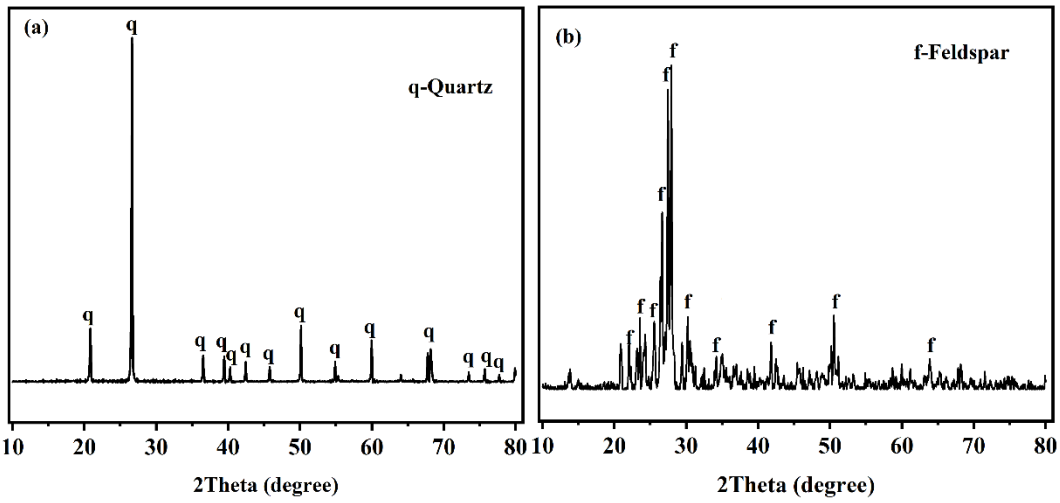

Fig. 1. XRD patterns of the (a) quartz and (b) feldspar specimens

Carboxymethyl starch sodium (CMS-Na) and poly(propylene glycol) bis(2-aminopropyl ether) (PEA, Mw≈400) were obtained from Aladdin Industrial Corporation in analytical grade. All solutions were prepared fresh before each experiment, with concentrations adjusted according to specific protocol requirements. Throughout the study, solutions were prepared using deionized water with a resistivity of 18.2 MΩ·cm. KBr of FTIR-grade was supplied by China National Pharmaceutical Group Co., Ltd., and analytical grade NaOH for pH adjustment was sourced from Aladdin Industrial Corporation. The molecular structures of the depressant (CMS-Na) and the collector (PEA) are shown in Fig. 2.

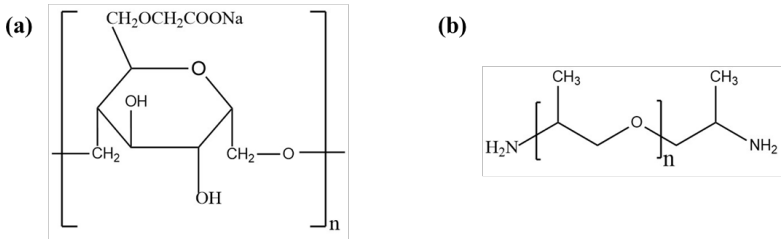

Fig. 2. The structure of CMS-Na (a) and PEA (b)

2.2. Methods

2.2.1. Flotation experiments

Micro-flotation experiments were conducted in a 40 cm^3 XFG-II mechanically agitated cell (Jilin Exploration Machinery Plant, China) at 1600 rpm. For each assay, the flotation cell was charged with 2.0 g of ore sample and deionized water to a total volume of 40 cm^3. The procedure followed the scheme outlined in Fig. 3. After 2 min pre-conditioning, the slurry pH was adjusted to values between 7 and 12 using NaOH. Depressant CMS-Na was then added at dosages of 0-50 mg/dm^3 and conditioned for 2 min, followed by introduction of the collector PEA at a fixed concentration of 4.0×10^{-4} mol/dm^3. Flotation was performed for 3 min. The suspension was conditioned for an additional 2 min before introducing the collector PEA. The flotation process was carried out for 3 min.

Artificial mixed minerals were prepared by blending feldspar and quartz in a 1:1 mass ratio. After flotation, the concentrates and tailings were dried, weighed, and assayed. Recoveries were calculated based on mass distribution and chemical analysis. Each condition was tested in triplicate, and average values are reported. Feldspar recovery ($\varepsilon_{F\text{-}C}$, %) was evaluated from Na_2O and K_2O content in the concentrate using Eq. (2), while quartz recovery ($\varepsilon_{Q\text{-}C}$, %) was calculated via Eq. (3). The K and Na concentrations were determined by atomic absorption spectrophotometry.

$$\varepsilon_{F-C} = \frac{\varepsilon_{Na_2O} + \varepsilon_{K_2O}}{2} \tag{2}$$

$$\varepsilon_{Q-C} = \frac{Q_C - \varepsilon_{F-C} \cdot Q_F}{Q_Q} \tag{3}$$

where ε_{Na2O} and ε_{K2O} represent the potassium albite (Na_2O) and feldspar (K_2O) flotation recoveries in the flotation concentrate, respectively. The mass terms Q_C (total concentrate), Q_F (feldspar), and Q_Q (quartz) were determined for the artificially mixed ore system.

The separation efficiency between quartz and feldspar was assessed using the Selectivity Index (SI). For the artificially blended mineral system, the SI was calculated according to Eq. (4) (Xu, 1998).

$$SI = \sqrt{\frac{\varepsilon_{Q-C}}{\varepsilon_{F-C}} \cdot \frac{\varepsilon_{F-T}}{\varepsilon_{Q-T}}} \tag{4}$$

where $\varepsilon_{F\text{-}T}$ and $\varepsilon_{Q\text{-}T}$ are the mass recovery indices of feldspar and quartz reporting to the tailings, respectively. A higher SI signifies more efficient separation of quartz from feldspar. All tests were conducted in triplicate, and average values are reported.

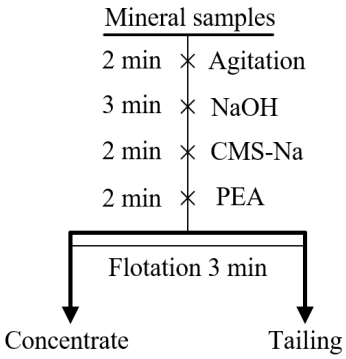

Fig. 3. Flotation procedure for single-mineral and their binary mixtures

2.2.2. Atomic absorption spectrophotometer

Sodium and potassium contents were quantified by atomic absorption spectrometry on an iCE 3500 instrument (Thermo Fisher Scientific, USA). To enable analysis, the samples were fully digested with a mixed HF-H_2SO_4 solution. After wavelength calibration with a copper lamp, the absorbances of Na and K were measured using an air-acetylene flame in a sulfuric acid medium, with detection at 766.5 nm and 589 nm, respectively.

2.2.3. Zeta potential measurements

The zeta potential measurements were conducted using a 90 Plus PALS dynamic light scattering instrument (Brookhaven, USA). A 0.5 g sample of pure mineral (< 5 μm) was dispersed in 100 cm^3 of 1.10^{-3} mol/dm^3 KCl solution, aged for 24 h, and then vigorously agitated to achieve homogeneity. Subsequently, 10 cm^3 of the suspension was diluted to 200 cm^3 with 1.10^{-3} mol/dm^3 KCl and conditioned for 10 min with the target concentration of CMS-Na or PEA. Approximately 1.5 cm^3 of the conditioned slurry was transferred to a sample cuvette for analysis.

2.2.4. Spectroscopic analyses

FTIR samples were prepared by simulating key flotation stages. The mineral suspensions were stirred for 10 min, collected, and vacuum-dried at 318 K for 12 h. Before analysis, the dried samples were finely ground and homogeneously blended with FTIR-grade KBr at a mass ratio of about 100:1, followed by pellet pressing. FTIR spectra were acquired on a Nicolet 6700 spectrometer (Thermo Scientific, USA) at 4 cm^{-1} resolution over 4000-400 cm^{-1} to examine the adsorption mechanism of PEA on the mineral surface.

Raman spectra of feldspar and quartz samples, both pre- and post-treatment with CMS-Na, were characterized using a LabRAM HR Evolution microscope (HORIBA, FR). The samples were prepared as described in the FTIR analysis. A 785 nm laser was employed for excitation, with spectra acquired across the 50–1200 cm^{-1} range.

Survey and high-resolution spectra using XPS analysis were acquired with a Nexsa spectrometer (Thermo Fisher, USA). All spectra were referenced to the C1s peak at 284.80 eV and processed using Advantage software (Thermo Fisher Scientific). The samples were prepared as described in the FTIR analysis.

3. Results and discussion

3.1. Effect of pH and CMS-Na dosage on flotation performance

The dependence of quartz and feldspar flotation recovery on pulp pH at 4.0×10^{-4} mol/dm^3 PEA is shown in Fig. 4. The recovery of quartz initially increased with rising pH, reaching over 90% at pH 9.0 and peaking at 92% at pH 10.0, before slightly declining at higher pH values. Feldspar recovery also showed a gradual increase, from approximately 20% at pH 7.0 to 45% at pH 10.0, followed by a slight decrease at pH 12.0. The optimal separation, with a recovery difference of about 56%, occurred at pH 9.0.

The effect of CMS-Na concentration on quartz and feldspar recovery is shown in Fig. 5, under constant conditions of 4.0×10^{-4} mol/dm^3 PEA and pH 9.0. The recovery of quartz remained stable and was unaffected by the addition of CMS-Na. In contrast, the recovery of feldspar initially decreases with increasing CMS-Na concentration, reaching its lowest point of 17.84% at 30 mg/dm^3 CMS-Na, before starting to increase. At this dosage, the floatability difference between the two minerals reached the largest value, 75.54%. Therefore, at the PEA dosage of 4.0×10^{-4} mol/dm^3 and pH 9.0, the CMS-Na dosage of 30 mg/ dm^3 was identified as the optimal dosage of the regulator for quartz-feldspar flotation separation.

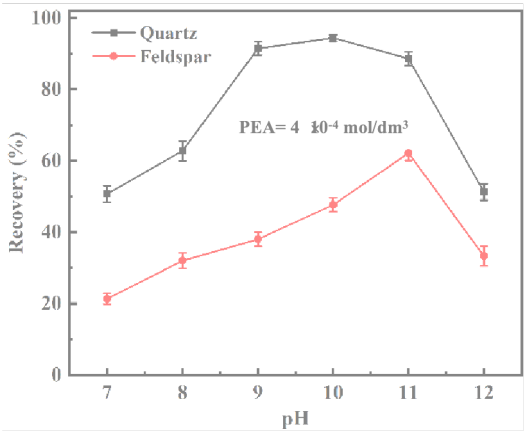

Fig. 5. Effect of CMS-Na concentration on quartz and feldspar recovery

3.2. Efficiency of quartz-feldspar flotation separation

The binary mixed-mineral flotation test serves as a verification test for flotation performance based on the single-mineral flotation test. Under the optimal conditions determined from single-mineral flotation, a

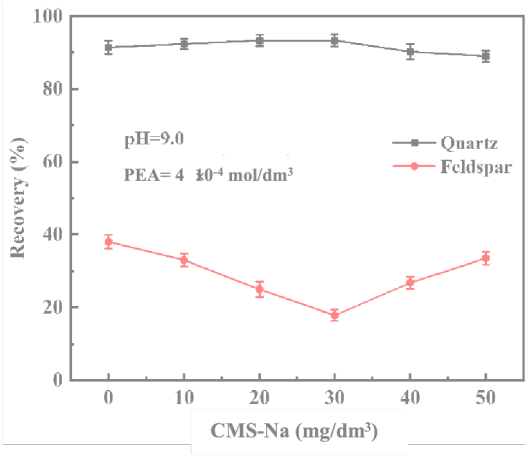

Fig. 4. Recoveries of quartz and feldspar as a function of pulp pH

binary mixture of quartz and feldspar (1.0 g each) was used to assess the selectivity of PEA. The corresponding data are summarized in Table 2. Without CMS-Na, the K_2O and Na_2O grades in the concentrate were 4.11% and 1.75%, respectively, slightly lower than in the raw mixed ore. The feldspar recovery was 56.70%, indicating that a significant portion of feldspar entered the concentrate. The SI value of 3.03 suggests a moderate separation effect, as PEA alone did not sufficiently suppress feldspar flotation. In contrast, the addition of CMS-Na substantially altered the flotation behavior. The K_2O and Na_2O grades in the concentrate dropped to 1.29% and 0.55%, respectively, reflecting CMS-Na's ability to reduce feldspar flotation into the concentrate. Feldspar recovery decreased sharply to 12.51%, showing that CMS-Na effectively suppressed feldspar flotation. The SI value increased significantly from 3.03 to 9.07, demonstrating a marked improvement in separation efficiency. Quartz recovery remained high in both conditions, with a slight decrease from 92.32% to 92.17% after adding CMS-Na. This minimal change suggests that CMS-Na has little to no adverse impact on quartz flotation, maintaining high recovery levels. The results highlight the role of CMS-Na as a selective depressant that enhances flotation separation by targeting feldspar while preserving quartz recovery. Overall, the data confirm that CMS-Na significantly improves the flotation separation of quartz and feldspar in the PEA system by selectively suppressing feldspar, increasing the SI value, and optimizing separation performance.

Table 2. Flotation performance of the quartz-feldspar mixture with and without CMS-Na

Conditions	Product	Yield (%)	Grades (%)			Recovery (%)		SI
			K_2O	Na_2O	SiO_2	Quartz	Feldspar	
pH: 9.0; PEA: 4×10-4 mol/dm3	Concentrate	74.51	4.11	1.75	88.29	92.32	56.7	3.03
	Tailings	25.49	9.43	3.8	74.08	7.68	43.3	
	Feed	100	5.47	2.27	84.67	100	100	
pH: 9.0; CMS-Na: 30 mg/dm3 PEA: 4×10-4 mol/dm3	Concentrate	52.34	1.29	0.55	96.20	92.17	12.51	9.07
	Tailings	47.66	10.04	4.16	72.00	7.83	87.49	
	Feed	100	5.46	2.27	84.67	100	100	

3.3. Surface interaction mechanisms: Zeta potential measurements

Fig, 6 shows the zeta potential of quartz and feldspar under the flotation test condition at pH 9.0, both exhibiting negative values. The zeta potential of quartz is -55.16 mV, reflecting its low isoelectric point and a significant gap from pH 9.0. When CMS-Na is applied alone on the quartz surfaces, its zeta potential

remains nearly unchanged (-53.80 mV), indicating weak CMS-Na adsorption on the quartz surface. In contrast, CMS-Na induces a distinct positive shift of 59.19 mV on feldspar, demonstrating strong CMS-Na adsorption capacity on feldspar surfaces.

Adsorption of PEA alone resulted in positive zeta potential shifts of +55.17 mV for quartz and +25.82 mV for feldspar. Consequently, PEA adsorption is stronger on quartz than on feldspar. With the co-action of CMS-Na and PEA, the zeta potential of quartz shifted positively by 46.88 mV, while that of feldspar shifted negatively by 3.30 mV, both relative to CMS-Na alone. This indicates that after CMS-Na adsorption on the quartz surface, PEA could still be adsorbed. However, CMS-Na adsorption is not conducive to PEA adsorption on the feldspar surface.

Moreover, compared to the zeta potential shifts caused by PEA alone, the combined presence of CMS-Na and PEA leads to relatively smaller changes for quartz, while feldspar experiences a more pronounced reduction in zeta potential shift. These findings suggest that CMS-Na selectively reduces PEA adsorption on feldspar while having little impact on quartz. This selective interaction enhances the flotation separation efficiency of quartz and feldspar in the PEA system.

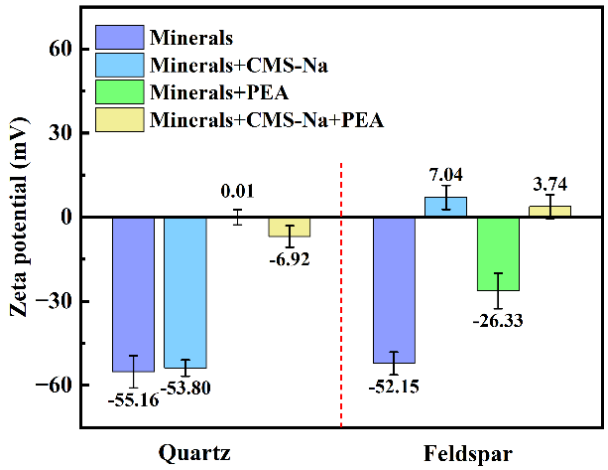

Fig. 6. Effect of CMS-Na and PEA on the zeta potential of quartz and feldspar

3.4. Adsorption mechanism analyzed by spectroscopic methods

In this study, FTIR was employed to characterize PEA adsorption due to the high infrared sensitivity of its polar amine groups. Conversely, Raman spectroscopy was selected for investigating CMS-Na to circumvent the intense Si−O background interference from quartz and feldspar in the infrared region (800−1200 cm^{-1}), thereby ensuring a more accurate identification of the depressant's characteristic vibrational modes on the mineral surfaces. FTIR tests were conducted to confirm the adsorption of PEA on quartz and feldspar surfaces, and the results are shown in Fig. 7. Fig. 7(a) shows the FTIR spectra of the quartz before and after PEA treatment. In the spectrum of pure quartz, peaks at 464 cm^{-1} (Si-O-Si asymmetric bending vibration), 694 cm^{-1} (Si-O symmetric bending vibrations), 789 cm^{-1} (Si-O symmetric stretching vibration), and 1109 cm^{-1} (asymmetric stretching vibration) were observed. Additionally, the peaks at 3302 cm^{-1} and 1621 cm^{-1} correspond to the stretching and bending vibrations of -OH, revealing the presence of silanol groups (Si-OH) on the quartz surface (Zhou, He et al. 2008, Liu, Liu et al. 2017). After PEA treatment, a new peak appears around 2970 cm^{-1}, attributed to the $-CH_3$ and $-CH_2$ stretching vibrations from PEA (Liu, Liu et al. 2017, Li, Lin et al. 2020). Other peaks remain largely unchanged, indicating no chemical adsorption. This suggests that PEA adsorbs physically on the quartz surface, likely through hydrogen bonding or electrostatic interactions.

Fig. 7(b) shows the FTIR spectra of the feldspar before and after PEA treatment. For pure feldspar, characteristic peaks appear at 1052 cm^{-1} (Si-O stretching vibration), 1007 cm^{-1} (Si(Al)-O bending vibration), 585 cm^{-1} (O-Si(Al)-O bending vibration), and 420 cm^{-1} (Si-O-Si bending vibration). After PEA treatment, a

new peak emerges around 2900 cm^{-1}, corresponding to the -CH_3 and -CH_2 stretching vibrations of PEA (Liu, Liu et al. 2017, Li, Lin et al. 2020). Similar to quartz, the original feldspar peaks remain unchanged, indicating that no chemical adsorption occurs. These findings confirm that PEA adsorbs on feldspar through physical interactions such as hydrogen bonding or electrostatic forces.

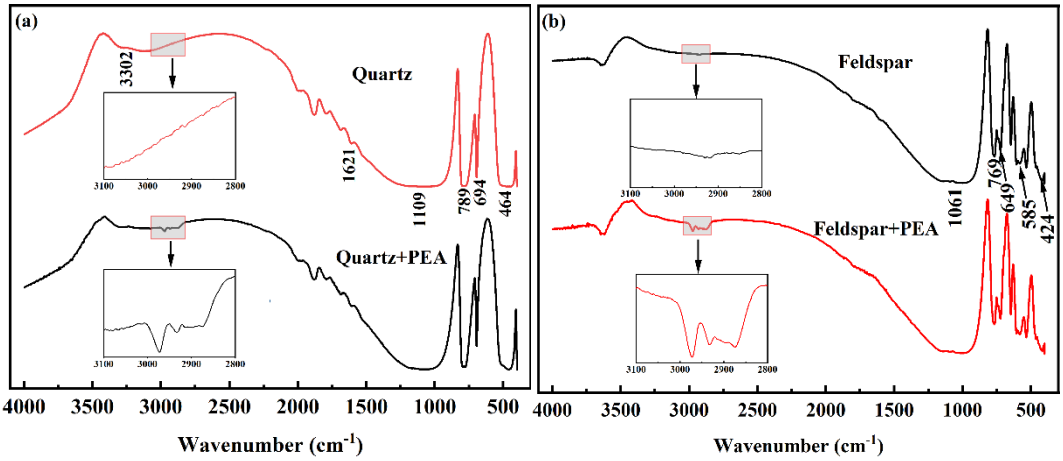

Fig. 7. Effect of PEA treatment on mineral FTIR spectra under pH 9.0 conditions

Raman spectroscopy was employed to investigate structural and compositional changes on the mineral surface prior to and following CMS-Na treatment, providing insights into the interaction between CMS-Na and the minerals.

Fig. 8(a) compares the Raman spectra of untreated and CMS-Na-treated quartz at pH 9.0. In the spectrum of pure quartz, prominent peaks are observed at around 128, 205, 263, 353, 464, and 1160 cm^{-1}, with the strongest peak at 464 cm^{-1} corresponding to the Si-O-Si symmetric stretching (De la Llave, Del Campo et al. 2019). No significant interaction between CMS-Na and quartz is evidenced by the largely unchanged Raman spectrum and absence of new characteristic peaks post-treatment.

The Raman spectra in Fig. 8(b) compare pure and CMS-Na-treated feldspar at pH 9.0. In pure feldspar, the bands at 500–510 cm^{-1} and 468–478 cm^{-1} are attributed to Si–O–Si (De la Llave, Del Campo et al. 2019) and Si–O–Al (Frost and Shurvell 1997) symmetric stretching vibrations, respectively. After CMS-Na treatment, noticeable changes in peak positions and intensities are observed. Notably, a strong enhancement at 159 cm^{-1}, indicative of hydrogen bonds, is present (Walrafen 1966). Additionally, a characteristic peak of C-O-C stretching at 760 cm^{-1} appears on the feldspar surface, confirming the formation of new species (Kaczmarska, Grabowska et al. 2018). The band at 812 cm^{-1} corresponds to a newly formed chemical bond (Al-O-C) through the coordination of carboxymethyl with Al. The band at 1097 cm^{-1} is basically associated with C-O-H stretching and bending vibrations (Yuen, Choi et al. 2009). These spectral changes suggest that CMS-Na strongly adsorbs onto the feldspar surface, consistent with the flotation results, whereas its interaction with quartz remains weak.

XPS measurements were utilized in this study to enhance our comprehension of the adsorption mechanism of CMS-Na on quartz and feldspar surfaces. The atomic compositions of the surfaces under investigation are presented in Table 3. Following the CMS-Na treatment, a marginal increase of 0.54% in oxygen content was observed on the quartz surface, rising from 56.75% to 57.29%. In contrast, a more substantial increase of 1.03% in oxygen content was registered on the feldspar surface, escalating from 56.05% to 57.08%. Furthermore, the sodium content on the feldspar surface exhibited a modest rise of 0.15% (from 1.47% to 1.62%), whereas no sodium was detected on the quartz surface. These findings suggest that feldspar possesses a greater affinity for CMS-Na adsorption compared to quartz.

The rise in oxygen and sodium levels is accompanied by a reduction in the concentrations of other elements, including Si, Al, and K. Specifically, on the surface of feldspar, there was a decrease of 0.28% in

silicon content, 0.83% in aluminum content, and 0.13% in potassium content, whereas the Si content on the surface of quartz decreased by 0.65%. This observation suggests that CMS-Na primarily binds to the aluminum sites of the feldspar surface, followed by the silicon sites. These findings support the conclusion that feldspar has a higher affinity for CMS-Na compared to quartz.

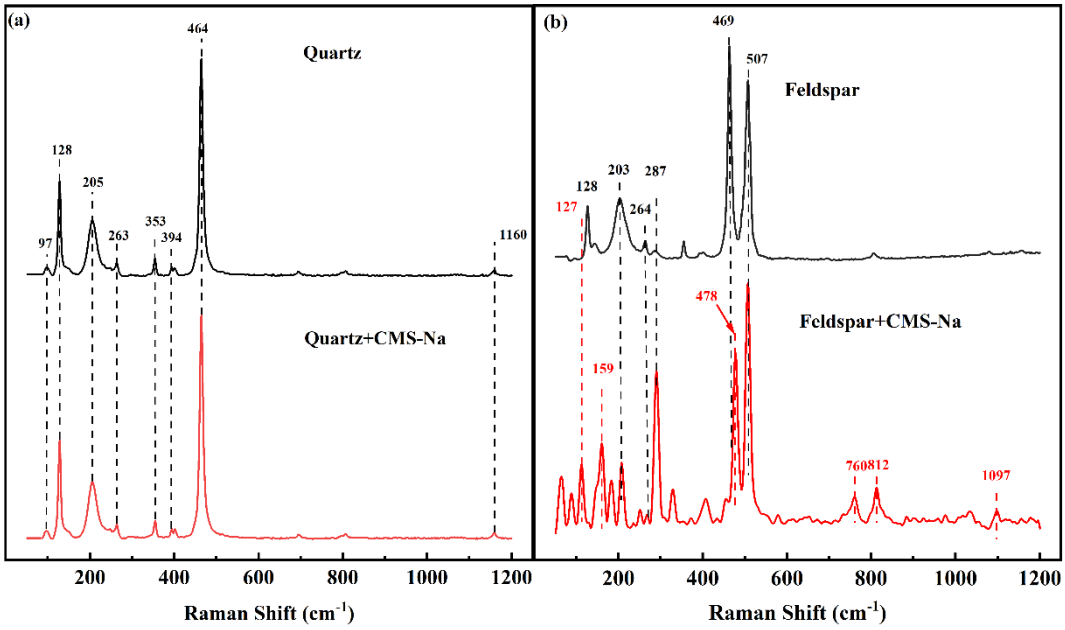

Fig. 8. Raman spectra of untreated and CMS-Na-treated minerals at pH 9.0

Table 3. Quantitative analysis of elemental distribution based on XPS

Sample	Atomic concentration, at%					
	C	Si	O	Al	K	Na
Quartz	14.61	28.64	56.75	-	-	-
Quartz+CMS-Na	15.72	27.99	57.29	-	-	-
Feldspar	14.59	16.24	56.05	9.04	2.61	1.47
Feldspar+CMS-Na	14.65	15.96	57.08	8.21	2.48	1.62

To evaluate changes in the surface chemical environment of feldspar following CMS-Na adsorption, the C1s, O1s, Si2p, and Al2p XPS spectra were analyzed (Fig. 9). As can be seen in Fig. 9(a), on the untreated feldspar surface, the C1s spectrum shows two peaks at 284.71 eV, attributed to adventitious carbon (Dong, Chen et al. 2017, Chen, Liu et al. 2021), and 285.23 eV, corresponding to sp^3 hybridized carbon (Mérel, Tabbal et al. 1998). After CMS-Na treatment, peaks appear at 284.81 eV and 286.12 eV after dividing, associated with C-O-H, C=O, C-C, and C-O-C bonds in the CMS-Na molecule. This indicates that CMS-Na adsorption on feldspar occurs primarily through hydrogen bonding and hydrophobic interactions (Xing, Hou et al. 2015, Pelissari, Ferreira et al. 2019).

The O1s peak-fitting results for feldspar are displayed in Fig. 9(b). For untreated feldspar, the O1s spectrum includes peaks at 530.72 eV (Si-O), 531.97 eV (surface hydroxyl groups), and 532.73 eV (Al-O) (Ohuchi, Ghose et al. 2006, Ren, Cai et al. 2015, A, B et al. 2020). After CMS-Na treatment, a new peak at 531.40 eV appears, attributed to C=O bonds in CMS-Na, suggesting CMS-Na's adsorption on the surface of feldspar (Yang, Chen et al. 2021). Additionally, the binding energy of the Al-O peak shifts from 532.73 eV to 532.84 eV, suggesting chemical interactions between CMS-Na and Al-sites.

The Si2p spectrum of untreated feldspar shows peaks at 102.17 eV, 102.78 eV, and 103.36 eV, as shown

in Fig 9(c). The peaks are attributed to surface Si-O, Si-OH, and Si-O-Si species on feldspar, respectively (Zelekew and Kuo 2016, Wang, Zhang et al. 2018, Idrees, Liu et al. 2019). After CMS-Na treatment, these peaks shift by +0.07, +0.19, and +0.32 eV, indicating changes in the chemical environment of Si due to CMS-Na adsorption. For the Al2p spectrum as shown in Fig. 9(d), the Al2p spectrum of untreated feldspar shows a peak at 74.05 eV, which is attributed to Al-O. Following CMS-Na modification, the peak of Al-O shifts to 74.18 eV, which confirms that Al is the primary active site for CMS-Na. A new peak at 75.04 eV appears, attributed to Al-O-C, suggesting that the carboxylate group (-COO^-) of the carboxymethyl group forms a coordinate bond with the Al-site.

Overall, Al sites are identified as the primary adsorption centers for CMS-Na, based on XPS evidence showing pronounced changes in their chemical environment alongside those of Si. These findings highlight the role of CMS-Na in forming hydrogen bonds and interacting chemically with active sites on feldspar.

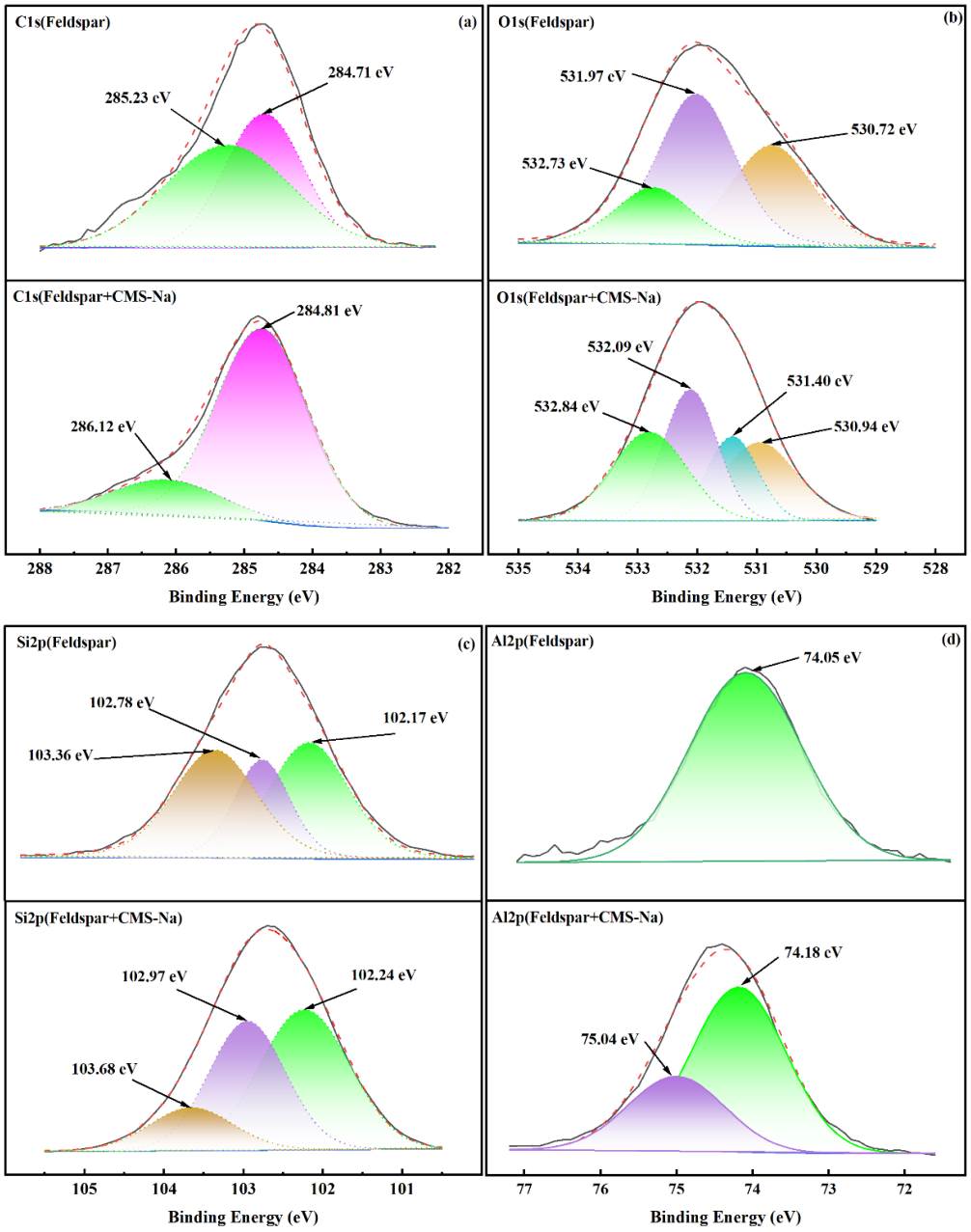

Fig. 9. XPS spectra of untreated and CMS-Na-treated feldspar: (a) C1s, (b) O1s, (c) Si2p, and (d) Al2p

To investigate the adsorption mechanism of PEA on quartz and feldspar surfaces, XPS analysis was conducted on untreated and PEA-treated samples. The XPS spectra of untreated quartz and feldspar show no N1s peak near 400 eV, confirming the absence of surface nitrogen (Fig. 10(a), (b)). In contrast, a distinct N1s peak appears in both minerals following PEA treatment (Fig. 10(c), (d)). This confirms that nitrogen originates from PEA adsorbed onto the mineral surfaces, providing direct evidence of PEA adsorption on quartz and feldspar.

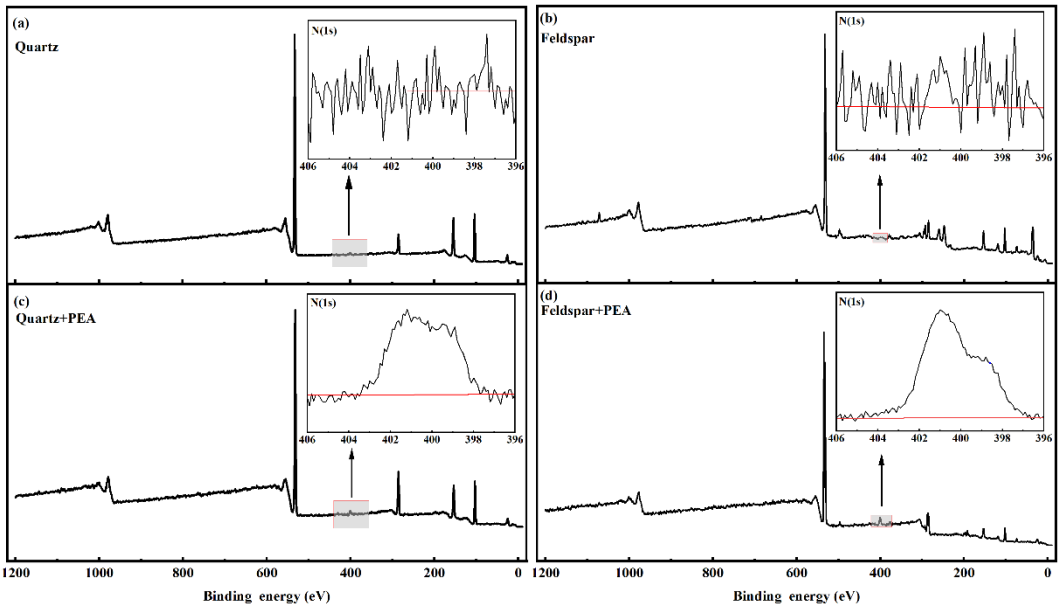

Fig. 10. Full XPS spectra of untreated minerals (a)-(b), and PEA-treated minerals (c)-(d)

Fig. 11 illustrates the fitted N(1s) peaks to further explore the adsorption mechanism of PEA on quartz and feldspar surfaces. As shown in Fig. 11(a) and (b), no distinct N(1s) peak is detected on the untreated quartz and feldspar surfaces. However, after PEA treatment, Fig. 11(c) and (d) reveal new N(1s) peaks with two components at approximately 401 eV and 399 eV. The peak near 401 eV corresponds to protonated nitrogen ($-NH_3^+$), while the peak at approximately 399 eV is assigned to deprotonated nitrogen ($-NH_2$) (Alagta, Felhoesi et al. 2008, Buckley and Parker 2013).

The two amino groups in PEA, each with a lone-pair electron, enable coordination with solution H^+ ions. In an alkaline environment, these groups can partially protonate to form $-NH_3^+$ (Jiang, Chen et al. 2022), allowing both $-NH_2$ and $-NH_3^+$ to coexist.

Upon crushing, the rupture of Si–O and Al–O bonds in quartz and feldspar generates undercoordinated sites ($-Si^+$, $-Al^+$, etc.). These sites undergo hydration to form $-Si-OH^-$ and $-Al-OH^-$ groups, resulting in negatively charged surfaces under alkaline conditions due to deprotonation. This aligns with their isoelectric points, which are approximately 2.0 for quartz and 1.5 for feldspar (Vidyadhar and Rao 2007, Gülgönül, Karagüzel et al. 2008).

The positively charged $-NH_3^+$ group in PEA binds to negatively charged $-Si-O^-$ or $-Al-O^-$ sites through electrostatic interactions, resulting in the 401 eV peak. Simultaneously, the uncharged $-NH_2$ group forms hydrogen bonds with -Si-OH or -Al-OH groups, producing the 399 eV peak. These interactions confirm that PEA adsorption on quartz and feldspar surfaces occurs via both electrostatic bonding and hydrogen bonding.

3.5. Mechanism of CMS-Na selective adsorption and separation

In summary, the findings indicate that CMS-Na effectively depresses feldspar while scarcely affecting quartz at low dosages. Fig. 12 illustrates the proposed interaction mechanism between CMS-Na and the

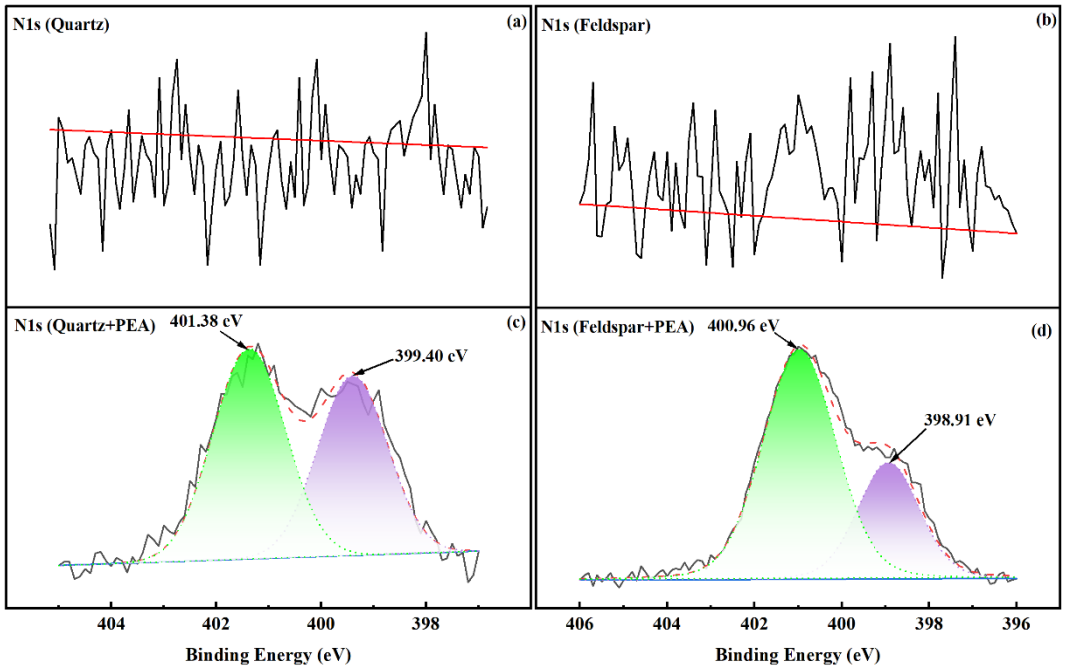

Fig. 11. Effect of PEA treatment on the XPS spectra of quartz (a) and feldspar (b)

quartz/feldspar surfaces. Compared to Si–OH sites, the Al–OH sites on feldspar are more reactive and serve as the primary adsorption sites for CMS-Na. Raman and XPS analyses suggest that the carboxymethyl groups in CMS-Na chemically interact with Al-sites and hydroxyl groups in CMS-Na physically interact with -Al-OH or -Si-OH on the feldspar. This interaction blocks reagent attachment to the feldspar surface, thereby reducing its floatability. Moreover, the multi-hydroxyl structure of CMS-Na further diminishes surface hydrophobicity. In contrast, its interaction with Si–OH sites on quartz is significantly weaker. As a result, CMS-Na adsorption on quartz is insufficient to block subsequent adsorption of activators and collectors, allowing quartz flotation to proceed unaffected.

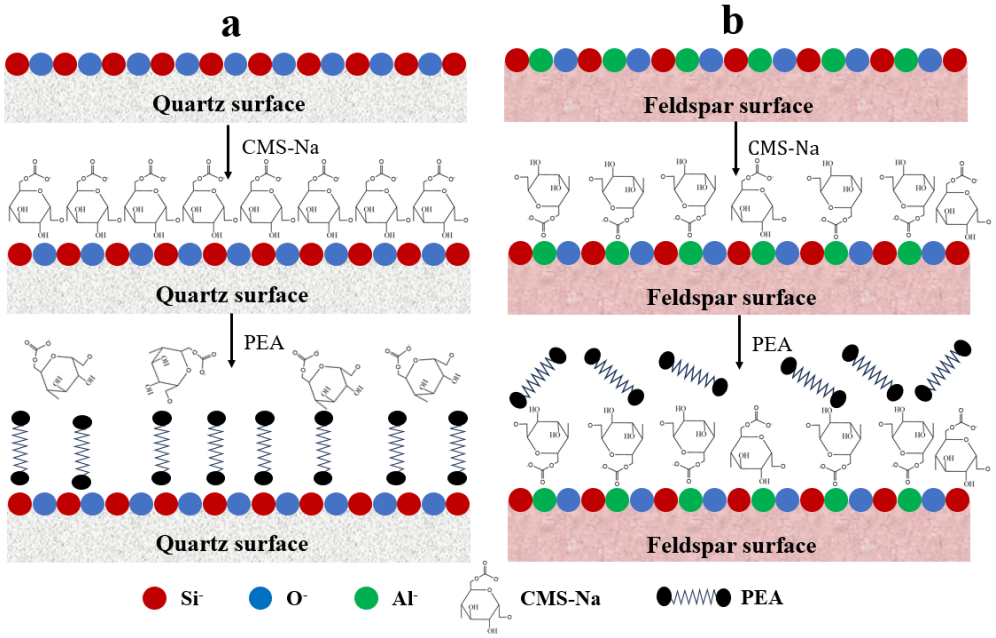

Fig. 12. Potential interaction modes of CMS-Na with quartz and feldspar surfaces

4. Conclusions

This work investigates the efficacy of a combined reagent scheme—CMS-Na depressant and PEA collector—for separating quartz from feldspar under weakly alkaline conditions. The results demonstrated that CMS-Na exhibited strong selective depression of feldspar while having minimal impact on quartz flotation. Micro-flotation tests confirmed that at an optimal CMS-Na dosage of 30 mg/dm^3 and pH 9.0, feldspar recovery decreased significantly to 12.51%, while quartz recovery remained high at 92.17%. The selectivity index (SI) increased substantially from 3.03 to 9.07, highlighting the enhanced separation efficiency achieved under these conditions.

Spectroscopic analyses, including FTIR, Raman, and XPS, revealed that CMS-Na selectively adsorbs onto feldspar surfaces mainly via coordination with Al-sites, with a small portion additionally forming hydrogen bonds with -Al-OH or -Si-OH, effectively suppressing its flotation. In contrast, the interaction between CMS-Na and quartz was weak, allowing the subsequent adsorption of PEA on quartz surfaces, which facilitated its flotation. Furthermore, XPS results confirmed that PEA adsorbed on both minerals, primarily through electrostatic and hydrogen bonding interactions. However, the presence of CMS-Na reduced PEA adsorption on feldspar, further enhancing the separation between the two minerals.

This work demonstrates an environmentally friendly and efficient approach to separating quartz and feldspar without the use of hazardous chemicals like hydrofluoric acid. The results highlight the potential industrial application of CMS-Na and PEA in flotation processes, offering a safer and more sustainable method for the comprehensive utilization of mineral resources.

Acknowledgments

This research was supported by the Open Foundation of State Key Laboratory of Mineral Processing under grant number BGRIMM-KJSKL-2025-25.

References

BERRISSOUL A., OUARHACH A., BENHIBA F., ROMANE A., ZARROUK A., GUENBOUR A., DIKICI B., DAFALI A., 2020. *Evaluation of Lavandula mairei extract as green inhibitor for mild steel corrosion in 1M HCl solution. Experimental and theoretical approach.* Journal of Molecular Liquids 313: 113493.

ALAGTA A., FELHOESI I., BERTOTI I., KALMAN E., 2008. *Corrosion protection properties of hydroxamic acid self-assembled monolayer on carbon steel.* Corrosion Science 50(6): 1644–1649.

BUCKLEY A. N., PARKER G. K., 2013. *Adsorption of n-octanohydroxamate collector on iron oxides.* International Journal of Mineral Processing 121: 70–89.

CHEN F. R., LIU Z., YU N., SUN H. X., GENG B. Y., 2021. *Constructing an interspace in MnO@NC microspheres for superior lithium ion battery anodes.* Chemical Communications 57(83): 10951–10954.

DE LA LLAVE V. F., DEL CAMPO A., FERNÁNDEZ J. F., ENRÍQUEZ E., 2019. *Structural insights of hierarchically engineered feldspars by confocal Raman microscopy.* Journal of Raman Spectroscopy 50(5): 741–754.

DONG Q. M., CHEN Y. Y., WANG L. L., AI S. S., DING H. M., 2017. *Cu-modified alkalinized g-C3N4 as photocatalytically assisted heterogeneous Fenton-like catalyst.* Applied Surface Science 426: 1133–1140.

FROST R. L., SHURVELL H. F., 1997. *Raman microprobe spectroscopy of halloysite.* Clays and Clay Minerals 45: 68–72.

GÜLGÖNÜL I., KARAGÜZEL C., ÇELIK M. S., 2008. *Surface vs. bulk analyses of various feldspars and their significance to flotation.* International Journal of Mineral Processing 86(1–4): 68–74.

IDREES M., LIU L., BATOOL S., LUO H. Z., LIANG J., XU B., WANG S., KONG J., 2019. *Cobalt-doping enhancing electrochemical performance of silicon/carbon nanocomposite as highly efficient anode materials in lithium-ion batteries.* Engineered Science 6: 64–76.

JIANG X. S., CHEN J., BAN B. Y., SONG W. F., CHEN C., YANG X. Y., 2022. *Application of competitive adsorption of ethylenediamine and polyetheramine in direct float of quartz from quartz–feldspar mixed minerals under neutral pH conditions.* Minerals Engineering 188: 107850.

KACZMARSKA K., GRABOWSKA B., SPYCHAJ T., ZDANOWICZ M., SITARZ M., BOBROWSKI A., CUKROWICZ S., 2018. *Effect of microwave treatment on structure of binders based on sodium carboxymethyl starch: FT-IR, FT-Raman and XRD investigations.* Spectrochimica Acta Part A: Molecular and Biomolecular Spectroscopy 199: 387–393.

LARSEN E., JOHANNESSEN N. E., KOWALCZUK P. B., KLEIV R. A., 2019. *Selective flotation of K-feldspar from Na-feldspar in alkaline environment.* Minerals Engineering 142: 105928.

LARSEN E., KLEIV R. A., 2016. *Flotation of quartz from quartz–feldspar mixtures by the HF method.* Minerals Engineering 98: 49–51.

LI J. W., LIN Y. H., SHI J., BAN B. Y., SUN J. F., MA Y., WANG F. M., LV W., CHEN J., 2020. *Recovery of high purity Si from kerf-loss Si slurry waste by flotation method using PEA collector.* Waste Management 115: 1–7.

LIU W. B., LIU W. G., WEI D. Z., LI M. Y., ZHAO Q., XU S. C., 2017. *Synthesis of N,N-bis(2-hydroxypropyl)laurylamine and its flotation on quartz.* Chemical Engineering Journal 309: 63–69.

MÉREL P., TABBAL M., CHAKER M., MOISA S., MARGOT J., 1998. *Direct evaluation of the sp^3 content in diamond-like-carbon films by XPS.* Applied Surface Science 136(1–2): 105–110.

MINAMI T., MAEDA S., HIGASA M., KASHIMA K., 2011. *In-situ observation of bubble formation at silicon melt–silica glass interface.* Journal of Crystal Growth 318(1): 196–199.

OHUCHI F. S., GHOSE S., ENGELHARD M. H., BAER D. R., 2006. *Chemical bonding and electronic structures of the Al_2SiO_5 polymorphs, andalusite, sillimanite, and kyanite.* American Mineralogist 91(5–6): 740–746.

PAN X. D., LI S. Q., LI Y. K., GUO P. H., ZHAO X., CAI Y. S., 2022. *Resource, characteristic, purification and application of quartz: a review.* Minerals Engineering 183: 107600.

PELISSARI F. M., FERREIRA D. C., LOUZADA L. B., SANTOS F. D., CORRÊA A. C., MOREIRA F. K. V., MATTOSO L. H., 2019. *Starch-based edible films and coatings: an eco-friendly alternative for food packaging.* In: Starches for Food Application, pp. 359–420.

REN J., CAI X., YANG H., GUO X., 2015. *Preparation and characterization of high surface area ZrO_2 aerogel modified by SiO_2.* Journal of Porous Materials 22(4): 973–978.

SANTOS M. F. M., FUJIWARA E., SCHENKEL E. A., ENZWEILER J., SUZUKI C. K., 2015. *Processing of quartz lumps rejected by silicon industry to obtain a raw material for silica glass.* International Journal of Mineral Processing 135: 65–70.

SHEN L. F., SUN N., XU R., SUN W., WANG L., 2023. *Adsorption mechanisms of activated surface of quartz and feldspar with mixed NaOL/DDA.* Separation and Purification Technology 314: 123501.

SUN N., WANG G. D., GE P., SUN W., XU L. H., TANG H. H., WANG L., 2023. *Selective flotation of quartz from feldspar using hydroxypropyl starch as depressant.* Minerals Engineering 195: 108022.

TENG Q., WANG H. J., 2021. *Effect of silicate bacteria on quartz flotation separation.* Separation Science and Technology 56(5): 982–990.

VIDYADHAR A., RAO K. H., 2007. *Adsorption mechanism of mixed cationic/anionic collectors in feldspar–quartz flotation system.* Journal of Colloid and Interface Science 306(2): 195–204.

VIELRA A. M., PERES A. E. C., 2007. *The effect of amine type, pH, and size range in the flotation of quartz.* Minerals Engineering 20(10): 1008–1013.

WALRAFEN G. E., 1966. *Raman spectral studies of the effects of urea and sucrose on water structure.* The Journal of Chemical Physics 44(10): 3726–3727.

WANG H. F., ZHANG G. W., HAO J., HE Y. Q., ZHANG T., YANG X., 2018. *Morphology, mineralogy and separation characteristics of nonmetallic fractions from waste printed circuit boards.* Journal of Cleaner Production 170: 1501–1507.

WANG L., LIU R. Q., HU Y. H., LIU J. P., SUN W., 2016. *Adsorption behavior of mixed cationic/anionic surfactants and their depression mechanism on the flotation of quartz.* Powder Technology 302: 15–20.

XING L. B., HOU S. F., ZHANG J. L., ZHOU J., LI Z., SI W., ZHUO S., 2015. *A facile preparation of three-dimensional N, S co-doped graphene hydrogels with thiocarbohydrazide for electrode materials in supercapacitors.* Materials Letters 147: 97–100.

XU M., 1998. *Modified flotation rate constant and selectivity index.* Minerals Engineering 11(3): 271–278.

YANG B., CHEN H., YANG Y., WANG L., LOU X., 2021. *Insights into the tribo-/pyro-catalysis using Sr-doped $BaTiO_3$ ferroelectric nanocrystals for efficient water remediation.* Chemical Engineering Journal 416: 128986.

YIN R. M., CHEN L. Z., HOU Q. L., LI J., LIU T. R., 2012. *Research on flotation mechanism of quartz using magnesium ion as activator.* Proceedings of the 2nd International Conference on Advanced Materials and Engineering Materials (ICAMEM 2012), Beijing, China.

YUEN S. N., CHOI S. M., PHILLIPS D. L., MA C. Y., 2009. *Raman and FTIR spectroscopic study of carboxymethylated non-starch polysaccharides.* Food Chemistry 114(3): 1091–1098.

ZELEKEW O. A., KUO D. H., 2016. *A two-oxide nanodiode system made of double-layered p-type Ag_2O@n-type TiO_2 for rapid reduction of 4-nitrophenol.* Physical Chemistry Chemical Physics 18(6): 4405–4414.

ZHOU Y. S., HE C. R., YANG X. S., 2008. *Water contents and deformation mechanism in ductile shear zone of middle crust along the Red River fault in southwestern China.* Science in China Series D: Earth Sciences 51(10): 1411–1425.